THE JOURNAL OF
PHYSICAL CHEMISTRY A

ARTICLE

pubs.acs.org/JPCA

Dicyano and Pyridine Derivatives of β-Carotene: Synthesis and Vibronic, Electronic, and Photophysical Properties

A. J. Cruz,[†] K. Siam,[‡] and D. P. Rillema*[,†]

[†]Department of Chemistry, Wichita State University, Wichita, Kansas 67260, United States

[‡]Department of Chemistry, Pittsburgh State University, Pittsburgh, Kansas 66762, United States

ABSTRACT: Density functional theory and time-dependent density functional theory calculations provide pictures of the molecular orbitals involved in the ground and excited states of two cyano derivatives of 8′-apo-β-caroten-8′-al synthesized via an acid−base-catalyzed Knoevenagel condensation reaction. Population analysis shows that the symmetry-allowed transition, S_0 (^1A_g) → S_2 (^1B_u) based on the C_{2h} symmetry is a HOMO (highest occupied molecular orbital) to LUMO (lowest unoccupied molecular orbital) $\pi \rightarrow \pi^*$ transition with electron densities located mostly on the polyene chain. Calculated and actual steady-state absorption spectra show similar features with low-energy peak maxima between 550 and 600 nm.

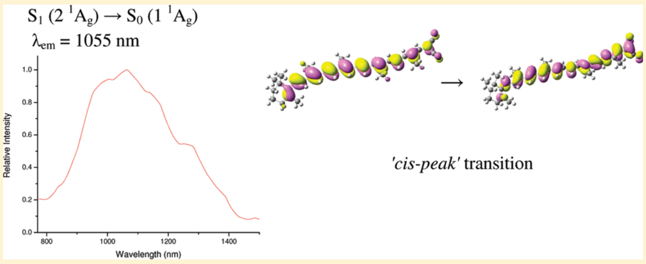

INTRODUCTION

Carotenoids play an important role in photosynthesis, particularly in their capacity to harvest light and initiate photosensitized energy transfer and electron transport in photosystems bound to cell membranes.[1−3] β-Carotenes, for instance, serve as antennas for absorbing light in spectral regions where chlorophylls do not absorb, and thus initiate photosynthesis.[4−10] In the past, group theoretical treatments based on the C_{2h} point group[4,5] for carotenes revealed that the electronic ground state is ^1A_g (S_0) in character, whereas the symmetry-allowed transition found in the visible region, responsible for pigment coloration in plant leaf tissues and light-harvesting properties in photosystems, is due to the population of a second excited state, ^1B_u (S_2),[2,4−22] shown in Figure 1. The $S_0 \rightarrow S_2$ transition has been well-characterized by steady-state absorption measurements conjoined with molecular orbital treatments.[4−22] The first ^1A_g (S_1) excited state has also been identified[1,11−13,23] and is known to lie between the ground state and the ^1B_u excited state. Previous studies involving carotenoids involved in the xanthophyll cycle showed that after the ^1A_g (S_0) → ^1B_u (S_2) transition, internal conversion occurs populating the S_1 excited state.[23,24] This process is the primary route in energy transfer and energy dissipation in carotenoid−chlorophyll systems.[23]

To date, this excited state has been characterized using low-temperature (77 K) emission studies[25] and two-photon excitation[26,27] and time-resolved infrared spectroscopy.[28−30] Triplet states have also been investigated previously by flash photolysis and pulse radiolysis and are known to be responsible for the photoprotection of plants by quenching triplet chlorophyll.[31,32]

Previously, the 7′,7′-dicyano-7′-apo-β-carotene was synthesized and AM1 (Austin-model 1) calculations were carried out to optimize the ground (1 ^1A_g), first excited state (2 ^1A_g), and second excited state (1 ^1B_u). Their relative charge densities were also reported and were localized on the C═C atoms in the polyene chain. The eigenvalues of the energy states were not reported.[33−35]

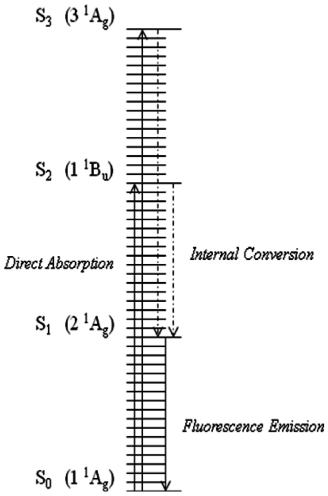

Figure 1. Energy diagram and photochemical processes in carotenoids (C_{2h} point group).

In this study, we reinvestigate the chemistry of 7′,7′-dicyano-7′-apo-β-carotene (**3**) synthesized via acid-catalyzed Knoevenagel condensation and a new cyanine derivative, 7′-cyano-7′-pyridyl-7′-apo-β-carotene (**2**), that can serve as antennas for attachment to transition metal complexes. Their photophysical

Received: July 7, 2010
Revised: December 20, 2010
Published: January 18, 2011

and vibronic properties have been examined. In a previous paper, we used semiempirical calculations to establish the properties of these states in short-chained systems.[33] Here, density functional theory (DFT) and time-dependent density functional theory (TDDFT) calculations have been employed to ascertain their spectral properties with respect to those determined experimentally. Population analysis was also performed and correlated with experimental results. Scheme 1 shows the structures of the β-carotene analogues. Relative energies of the S_1 state in carotenoids involved in the xanthophyll cycle have been identified indirectly by fluorescence studies and observed in the near-IR region.[1,23,28−30]

Scheme 1. Chemical Structure of Naturally Occurring 8′-Apo-β-caroten-8′-al (1) and Its Derivatives

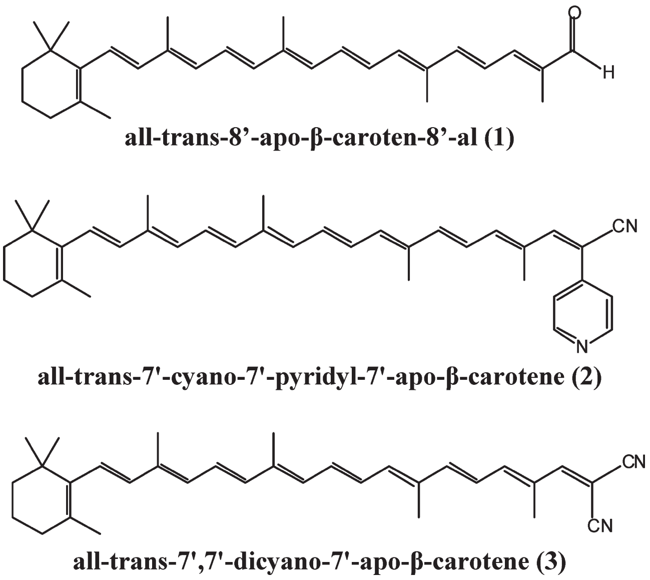

EXPERIMENTAL SECTION

Materials. The compound all-*trans*-8′-apo-β-caroten-8′-al (**1**) was obtained from Sigma. Malononitrile was obtained from Fluka; the compound 4-pyridyl acetonitrile monohydrochloride was purchased from Acros Scientific. Propionic acid and ammonium carbonate were purchased from Aldrich. Dried benzene, ethyl ether, HPLC grade methanol, chloroform, methylene chloride, and Optima grade acetonitrile for UV—vis spectral determinations were purchased from Fisher Scientific. IR grade potassium bromide salt used as a pellet for infrared spectral analysis was obtained from Aldrich. Sulfur powder used as standard to calibrate the Fourier transform (FT) Raman spectrometer was provided by Thermo Nicolet. A 4:1 ethanol/methanol solution was prepared and used as solvent for near-IR emission study.

*Preparation of All-trans-7′-cyano-7′-pyridyl-7′-apo-β-carotene (**2**).* The following preparation was performed under an argon atmosphere. All-*trans*-8′-apo-β-caroten-8′-al (103.3 mg, 2.23×10^{-4} mol) was placed in a 10 mL round-bottom flask. The compound was then dissolved in benzene and was allowed to stir for 5 min. After the solid dissolved, 4-pyridylacetonitrile monohydrochloride (58.3 mg, 5.30×10^{-4} mol) and ammonium carbonate (98.6 mg, 1.03×10^{-3} mol) were added to the solution and the reaction was allowed to stir for about 5 min. Then, 1.00 mL of propionic acid was added dropwise into the solution. After all the reagents were added, the reaction was refluxed overnight with its temperature regulated at approximately 70 °C.

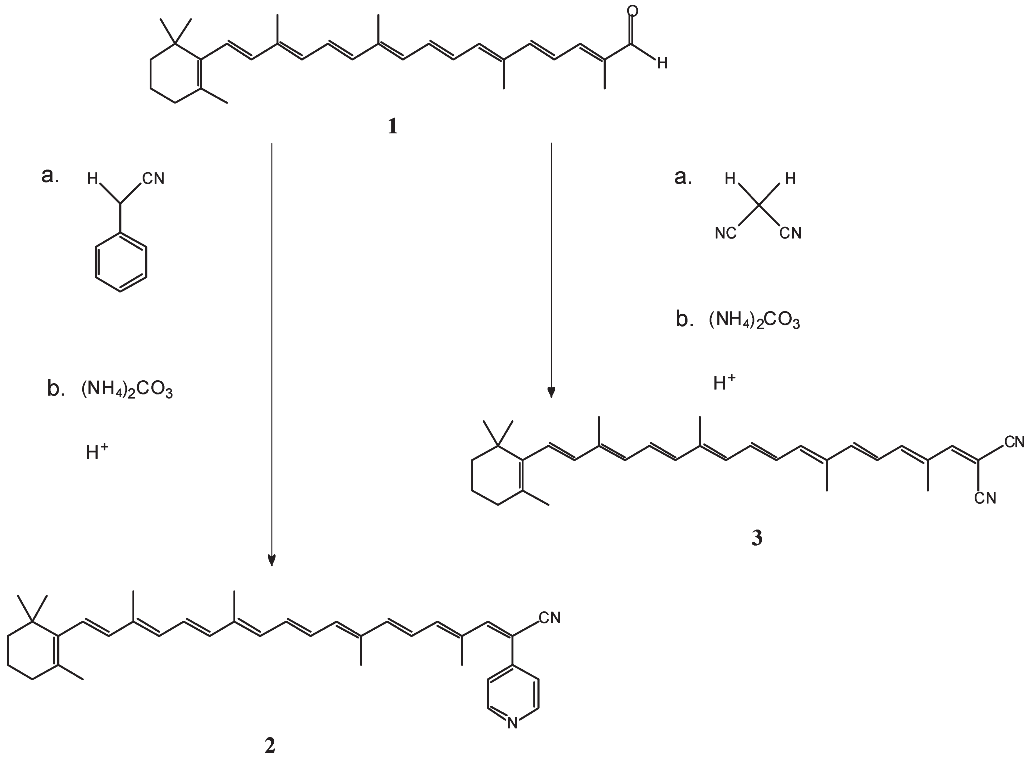

Figure 2. Knoevenagel condensation of 8′-apo-β-caroten-8′-al with 4-pyridylacetonitrile monohydrate and malononitrile.

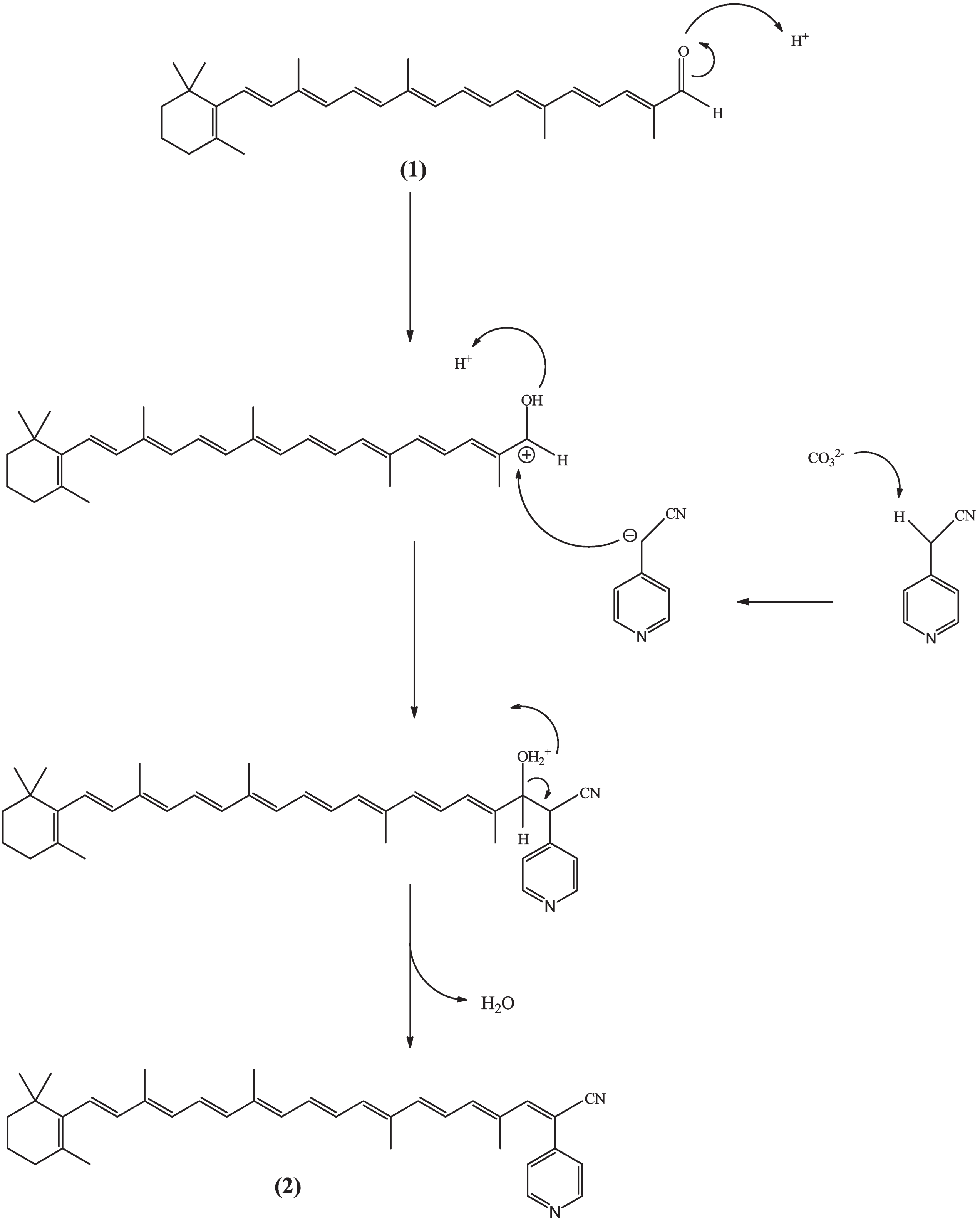

Figure 3. Mechanism for the acid- and base-catalyzed Knoevenagel condensation of 8′-apo-*β*-caroten-8′-al with 4-pyridylacetonitrile monohydrate.

Then, the reaction was allowed to cool in an ice bath, and the solvent was removed by lyophilization yielding a red-orange solid which was redissolved in chloroform and subjected to column chromatography through an oven-dried neutral alumina (∼10.0 g) stationary phase. The mobile phase used was 7:1 chloroform/methylene chloride. The first and final fractions were discarded, whereas the middle fractions were examined on thin-layer chromatography (TLC) plates for purity. The pure fractions were combined, and the solid was recovered after freeze-drying the solution to remove the solvent. The purple compound was dried

Table 1. Vibrational Stretching Frequencies (cm^{-1}) of CN and Polyene Groups

compound	functional group	experimental: (infrared)	experimental: (Raman)
8′-apo-β-caroten-8′-al, **1**	C=O stretch	1669	na
	−C=C− skeletal	1524	1521
		1567	
		1610	
	=C−H in-plane bending	na	1148
all-*trans*-7′-cyano-7′-pyridyl-7′-apo-β-carotene, **2**	CN stretch	2201	2266
	−C=C− skeletal	1406	na
		1510	
		1546	
	=C−H in-plane bending	na	1232
	polyene −CH$_3$ stretch	2924	na
all-*trans*-7′,7′-dicyano-7′-apo-β-carotene, **3**	CN stretch	2205	na
	−C=C− skeletal	1400	
		1504	1506
		1546	
	=C−H in-plane bending	na	1164
	polyene −CH$_3$ stretch	2962	na

in a vacuum oven and was stored in a desiccator. Color: purple, 82%. Anal. Calcd for C$_{37}$H$_{44}$N$_2$: C, 85.98; H, 8.50; N, 5.40. Found: C, 86.01; H, 8.19; N, 4.25. IR (KBr pellet, cm^{-1}): (CN) 2201 m, (−C=C−) 1503 sh, 2924 w. Raman (solid, cm^{-1}): (CN) 2266, (−C=C−H) 1232.

*Preparation of All-trans-7′,7′-dicyano-7′-apo-β-carotene (**3**).* All-*trans*-8′-apo-β-caroten-8′-al (101.2 mg, 2.18 × 10^{-4} mol) was placed in a 10 mL round-bottom flask. The compound was then dissolved in benzene and allowed to stir for 5 min. After dissolution, malononitrile (58.3 mg, 5.30 × 10^{-4} mol) and ammonium carbonate (98.6 mg, 1.03 × 10^{-3} mol) were added to the solution and the reaction was allowed to stir further for about 5 min. Then, 1.00 mL of propionic acid was added dropwise into the solution. After all the reagents were added, the reaction was refluxed overnight with its temperature regulated at approximately 70 °C. Then, the reaction was allowed to cool in an ice bath and the solvent was removed by lyophilization. The purple-black solid was redissolved in chloroform and was subjected to column chromatography through an oven-dried neutral alumina (~10.0 g) stationary phase. The mobile phase used was 7:1 chloroform/methylene chloride. The first and final fractions were discarded, whereas the middle fractions were examined for purity on TLC plates. After combining the fractions, the solid was recovered after freeze-drying the solution to remove the solvent. The dark compound was placed in a vacuum oven to dry. Color: black, 85%. Anal. Calcd for C$_{33}$H$_{40}$N$_2$: C, 85.28; H, 8.68; N, 6.03. Found: C, 85.09; H, 8.41; N, 5.86. IR (KBr pellet, cm^{-1}): (CN) 2205 m, (−C=C−) 1501 sh, 2962 w. Raman (solid, cm^{-1}): (−C=C−) 1506, (−C=C−H) 1164

Measurements. Infrared spectra were obtained using Perkin-Elmer model 1600 FT-IR and Nicolet Avatar model FT-IR spectrophotometers. All samples were prepared as potassium bromide pellets. Raman spectra were obtained using a Thermo Nicolet FT Raman module spectrophotometer. The Nicolet instruments were accompanied by Omni software programs. Proton (^{1}H) and carbon (^{13}C) NMR spectra were obtained using Varian Mercury 300 MHz and Varian Inova 400 MHz FT NMR spectrometers (internal standard, TMS). Ultraviolet spectra were obtained using a Hewlett-Packard model 8452A diode array spectrophotometer interfaced with an OLIS software program. Elemental (C, H, and N) analysis was performed by MHW Laboratories. Near-IR emission was carried out using a SPEX Nanolog spectrometer. Samples for emission studies were degassed via the freeze−pump−thaw method[36] with the absorbance set at 0.1 λ_{ex} = 519 nm.

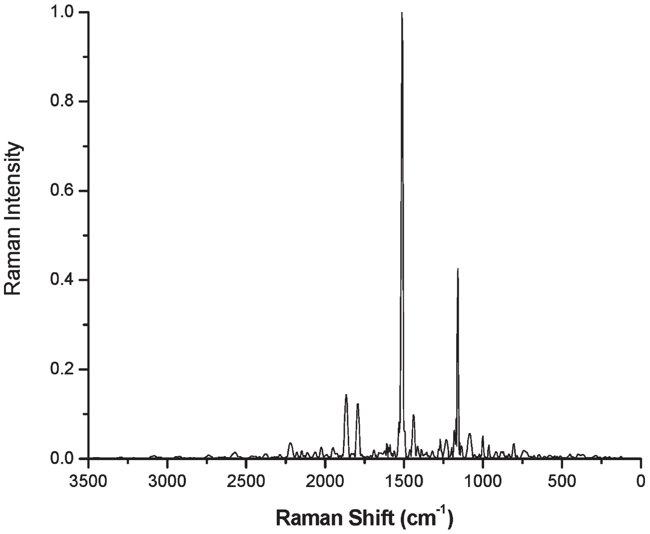

Figure 4. Raman spectrum of 8′-apo-β-caroten-8′-al (solid).

Calculations. Calculations were effected using Gaussian ’03 (rev. B.03)[37] for UNIX. The molecules were optimized using Becke’s three-parameter hybrid functional B3LYP[38] with the local terms[39] of Lee, Yang, Parr and the nonlocal term[40] of Vosko, Wilk, and Nassiar. The basis set 6-311G** was chosen for all atoms, and the geometry optimizations were all ran in the gas phase. TDDFT[41−47] calculations were employed to produce a number of singlet excited states[48] in the gas phase based on the optimized geometry. Simulated absorption spectra were generated using the Gauss sum 2.2 software package for the TDDFT data.

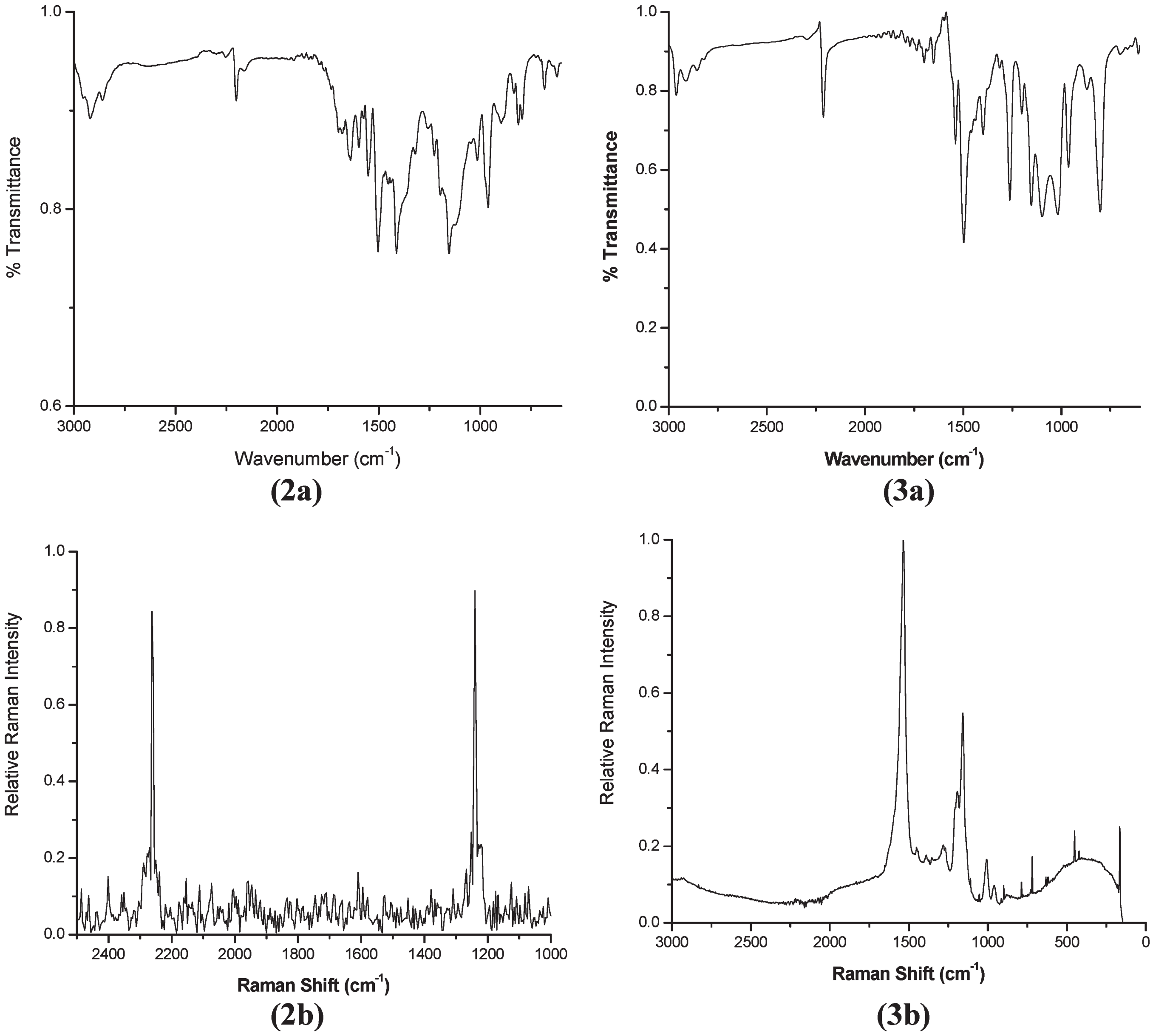

(2a)

(3a)

(2b)

(3b)

Figure 5. Infrared spectra: **2a** and **3a** (solid). Raman Spectra: **2b** and **3b** (solid).

RESULTS AND DISCUSSION

Synthesis. The preparation of **2** and **3** followed the Knoevenagel[49,50] reaction which involved the condensation of the aldehyde, 8′-apo-*β*-caroten-8′-al, with substrates lacking α-hydrogen atoms adjacent to the coupling site. This criterion is required to enhance the acidity of the methylene ($-CH_2-$) protons. Traditionally, this condensation reaction is catalyzed using only a weak base such as piperidine or $NaNH_2$.[49] In our case, we used simultaneous base- and acid-catalyzed condensation reactions to enhance the yield. The base catalyst used was NH_4CO_3, whereas the acid catalyst chosen was propionic acid (CH_3CH_2-COOH). The reaction scheme is shown in Figure 2.

The mechanism of formation of the pyridyl adduct is presented in Figure 3. This can be extended to the dicyano derivative. In this reaction, the base catalyst was added first to the reaction mixture to neutralize the hydrochloride and to deprotonate one of the methylene ($-CH_2-$) protons. Then, the weak acid catalyst was added to protonate the carbonyl oxygen generating the carbonyl carbocation necessary to initiate the condensation reaction.

Vibrational Properties. The infrared and Raman spectral data of carotene reactant and products are listed in Table 1. The Raman spectrum of 8′-apo-*β*-caroten-8′-al is shown in Figure 4. The IR spectrum of 8′-apo-*β*-caroten-8′-al for skeletal vibrations was consistent with previously published results.[28] Both IR and Raman spectra of the products are shown in Figure 5. As found in Table 1, the carbonyl ($C{=}O$) stretch of 8′-apo-*β*-caroten-8′-al is IR-active but not Raman-active. This stretching frequency occurs at 1669 cm^{-1}. Results show that the Raman behavior of the long-chained derivatives follows the same trend as their short-chained counterpart.[34] The Raman scattering in **2** is a little weaker than that of **3**. In the case of the pyridine adduct, the CN stretching frequency is both IR- and Raman-active with the latter having a higher energy than its cyano-pyridine counterpart. Their energies are found at 2201 and 2266 cm^{-1}, respectively. As expected,

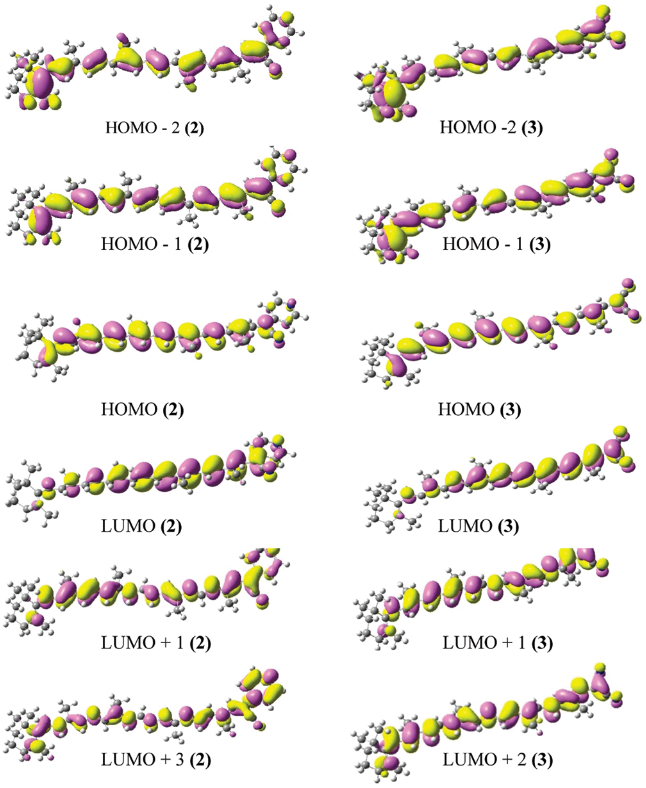

Figure 6. Orbital pictures of selected states involved in optical transition in **2** and **3**.

Table 2. Percentage of Electronic Distribution in Carotene Derivatives

states:	all-*trans*-7′-cyano-7′-pyridyl-7′-apo-β-carotene, **2**	all-*trans*-7′,7′-dicyano-7′-apo-β-carotene, **3**
LUMO + 3	5 (chain) 0 (β-ring) 90 (CN) 5 (pyridyl)	78 (chain) 18 (β-ring) 4 (CN)
LUMO + 2	77 (chain) 7 (β-ring) 1 (CN) 15 (pyridyl)	87 (chain) 8 (β-ring) 5 (CN)
LUMO + 1	83 (chain) 3 (β-ring) 10 (CN) 3 (pyridyl)	89 (chain) 3 (β-ring) 7 (CN)
LUMO	88 (chain) 1 (β-ring) 7 (CN) 4 (pyridyl)	91 (chain) 1 (β-ring) 8 (CN)
HOMO	90 (chain) 6 (β-ring) 2 (CN) 2 (pyridyl)	90 (chain) 7 (β-ring) 3 (CN)
HOMO − 1	76 (chain) 16 (β-ring) 5 (CN) 3 (pyridyl)	74 (chain) 20 (β-ring) 6 (pyridyl)
HOMO − 2	57 (chain) 35 (β-ring) 6 (CN) 2 (pyridyl)	56 (chain) 38 (β-ring) 6 (pyridyl)
HOMO − 3	62 (chain) 29 (β-ring) 8 (CN) 2 (pyridyl)	70 (chain) 24 (β-ring) 7 (pyridyl)

Table 3. UV−Visible Data of the $S_0\ {}^1A_g \rightarrow S_2\ {}^1B_u$ Transition in 1, 2, and 3

compound:	E (λ_{max}) (exptl)[a]	ε (M^{-1} cm^{-1})	E (λ_{max}) (calcd)
1	448	7.11×10^5	541
2	517	8.00×10^4	609
3	519	6.33×10^4	625

[a] Dried acetonitrile.

the −C═C− skeletal stretching frequencies of the cyano products are lowered compared to those of 8′-apo-β-caroten-8′-al. The −C═C− IR stretch in the cyano-pyridyl adduct can be found at 1503 cm^{-1}. In case of the dicyano derivative, this stretching frequency is both IR- and Raman-active and located at 1501 and 1506 cm^{-1}, respectively. The polyene $-CH_3$ stretch of the pyridine and dicyano adduct are found at 2924 and 2962 cm^{-1}, respectively.

■ CALCULATIONS (DFT/TDDFT)

Molecular Orbitals. The highest occupied molecular orbitals (HOMOs) and lowest unoccupied molecular orbitals (LUMOs) of the cyano-pyridyl adduct determined by DFT calculations are shown in Figure 6. The electron density is somewhat shifted from the HOMO to the LUMO toward the pyridyl ring even though the majority of the electron density is localized on the polyene chain. This trend is similar to the short-chained counterpart, as reported previously.[36]

The same electron density shift can also be observed in the nature of the HOMO/LUMO orbitals of the dicyano-carotenoid derivative as shown in Figure 6. Here the shift in the electron density is even greater from the β-ring and moves toward the nitrile groups than for cyano-pyridine derivative.

Population Analysis. Table 2 lists the population analysis data and the percentage electronic distribution of some selected states in **2** and **3** as shown in Figure 6. All calculations were effected using TDDFT. Results show similar trends as their short-chained counterparts.[36] The HOMO is predominantly polyene in character with 90% occupancy in both **2** and **3**. The most remarkable result is that both have equal electronic densities in the conjugated chain, where in dicyano's case, the β-ring and CN groups do not play an important contribution. The same trend was observed in the case of the LUMO of both **2** and **3**. Although the LUMO character lies on the polyene chain, the electron density of the LUMO in **2** is distributed throughout the molecule and is shifted to the newly condensed group, 4% pyridyl group contribution.

This pyridyl group plays an important role in hosting the excited electron. In some cases the methyl groups of the polyene chain have minor contributions in one of the states such as that

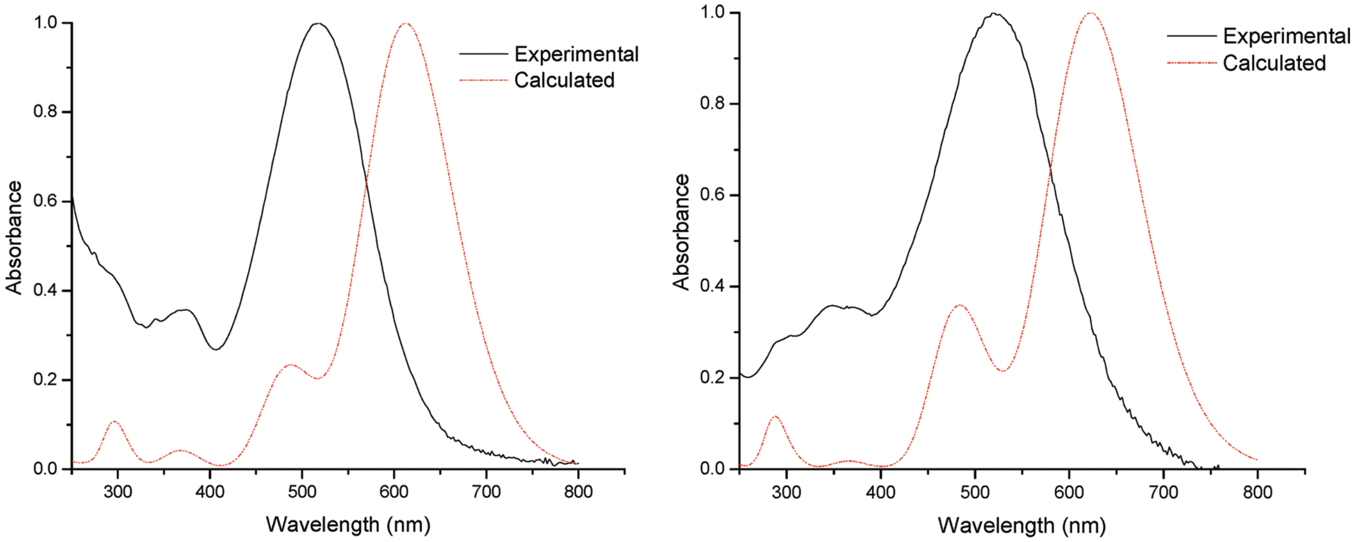

2 **3**

Figure 7. Experimental and calculated UV−vis data for **2** and **3**.

Table 4. Calculated UV−Visible Data for 2 and 3

2			3		
λ (nm)	F	major contributors	λ (nm)	F	major contributors
612	3.2580	HOMO → LUMO	622	2.9117	HOMO → LUMO
486	0.7496	HOMO − 1 → LUMO HOMO → LUMO + 1	483	1.0436	HOMO − 1 → LUMO HOMO → L + 1
372	0.1123	HOMO − 2 → LUMO HOMO − 1 → LUMO + 1 HOMO → LUMO + 1	369	0.0422	HOMO − 2 → LUMO HOMO − 1 → LUMO + 1 HOMO → LUMO + 1
309	0.0851	HOMO − 3 → LUMO HOMO − 2 → LUMO + 1 HOMO → LUMO + 2 HOMO → LUMO + 4	352	0.0132	HOMO − 3 → LUMO HOMO − 2 → LUMO HOMO − 1 → LUMO + 1
296	0.1509	HOMO − 2 → LUMO + 1 HOMO → LUMO + 3	306	0.0653	HOMO − 2 → LUMO + 1 HOMO → LUMO + 2
294	0.1115	HOMO → LUMO + 3	294	0.0152	HOMO − 4 → LUMO
287	0.0399	HOMO − 1 → LUMO + 2 HOMO → LUMO + 4	287	0.2894	HOMO − 2 → LUMO + 1 HOMO − 1 → LUMO + 2 HOMO → LUMO + 2
264	0.0266	HOMO − 7 → LUMO HOMO − 3 → LUMO + 1	277	0.0262	HOMO − 1 → LUMO + 2 HOMO → LUMO + 3

observed in HOMO − 2. In the latter case, the π-bonding interaction observed in retinoids arises every third atom of the polyene chain. All low-lying LUMO orbitals in **2** have major contributions from the pyridyl ring. The electronic distributions of other low-lying HOMO and LUMO orbitals are pictured in Figure 6. The electronic density distribution in the higher LUMOs of **3** is localized mostly on the polyene chain where the cyano groups have less effect on the π-conjugation. However, as the electron density shifts toward the dicyano group, the β-ring electronic density depletes as one goes from the LUMO to the higher LUMO orbitals. For instance, the β-ring has a 1% contribution in the electron density of its LUMO and an 18% contribution in the LUMO + 3.

Electronic Spectra. The UV−vis spectral data of the compounds are given in Table 3. Both experimental and calculated data showed bathochromic shifts in the visible region of the absorption spectrum, as expected, with respect to the starting 8′-apo-β-caroten-8′-al derivative. For the cyano-pyridine derivative, $\lambda_{\max}$ was shifted by 69 nm from 448 to 517 nm. Unlike the short-chained version,[34] $\lambda_{\max}$ of the dicyano derivative did not shift much relative to the pyridyl adduct, which is observed at 519 nm. However, a similar bathochromic trend is observed with respect to the energy positions of the $\lambda_{\max}$ in the visible spectrum. This is due to the lengthening of the polyene chain (1-D box). After condensation, a new double bond was generated between the carbonyl carbon of the retinal and the methylene groups of

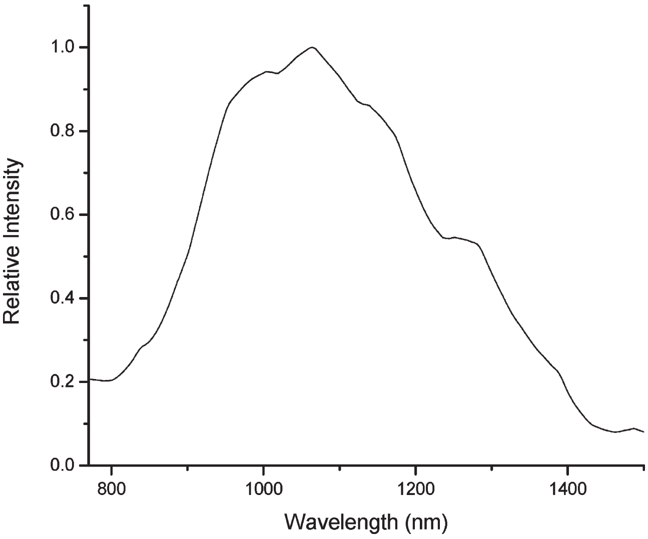

Figure 8. Near-IR emission spectrum of **3** in 4:1 EtOH/MeOH.

CN−C−py (for **2**) and CN−C−CN (for **3**). The experimental molar extinction coefficients are also tabulated in Table 3. Results gave a value of 8.00×10^4 M^{-1} cm^{-1} for **2** and 6.33×10^4 M^{-1} cm^{-1} in **3**. The UV−vis spectra of **2** and **3** are shown in Figure 7.

The theoretical UV−vis absorption data of **1**, **2**, and **3** were determined using TDDFT calculations and are overlaid with the actual electronic spectra (Figure 7). The calculated λ_{max} are also listed in Table 3. Similar to the short-chained derivatives,[34] a hypsochromic shift was observed in the actual electronic spectra of the carotenoid derivatives compared to the simulated ones. However, in the latter case, the absorption spectra in gas phase appear approximately 100 nm more red-shifted compared to the ones in liquid solution. The lowest energy $\pi \to \pi^*$ transitions in **2** underwent an actual blue-shift from 609 nm in gas phase to 517 nm in acetonitrile solution. For **3**, the shift was from 625 to 519 nm in solution. Calculations revealed that the lowest energy transition occurred from the HOMO to LUMO in both **2** and **3**, similar to the ones observed in their retinoid counterparts.[31] Experimentally, a weak absorption band was also observed for both cases appearing in the UV region (Figure 7). Overall, the features in both experimental and theoretical spectra are similar despite the energy shift observed. The shift is often observed due to the gas-phase calculations compared to the experimental results in solution.

The assignment of these transitions can be related to those determined from group theoretical treatment[4−22] given in Figure 1 with the A_g and B_u symmetry orbital labels applied to both cyano carotenoid derivatives to describe the nature of the $\pi \to \pi^*$ band (S_0 $^1A_g \to S_2$ ^1B_u). As expected, the $\pi \to \pi^*$ located on the polyene chain is the major contributor to the lowest energy transition. The HOMO of **2** (Figure 6) shows the electron density as located on the polyene chain with a small contribution from the β-ring, whereas the LUMO shows some electron density of the polyene chain extending toward the pyridyl group.

The HOMO of **3** is spread out over the polyene chain, the dicyano group, and the β-ring. Some p-orbital contribution in the case of the methylene carbon is also observed. Its LUMO on the other hand is less distorted compared to its retinoid derivative and is very distinctive of polyene chain π^*-orbital with a small contribution from the dicyano groups.

As also shown in Figure 7, the simulated UV−vis spectra obtained using TDDFT calculations gave rise to four distinct theoretical bands in **2**, whereas three bands were calculated for **3**. Table 4 lists selected transitions, their corresponding oscillator strengths, and the major molecular orbitals that contribute in each transition. As expected, the HOMO to LUMO transition of **2** (S_0 $^1A_g \to S_2$ ^1B_u) has the highest oscillator strength (f = 3.2580), in agreement with its high molar extinction coefficient, and is the predominant peak calculated in the UV−vis spectrum with its maximum centered at 609 nm. A theoretical peak located at 486 nm with oscillator strength of 0.75 involves the following transitions: HOMO − 1 → LUMO and HOMO → LUMO + 1. The other calculated peaks merge pairwise into the peaks shown in Figure 7. For example, the peaks at 372 and 296 nm appear as one peak. The calculated peak at 296 and 294 nm gave an average oscillator strength of 0.13. Under this band lie the following transitions: HOMO − 2 → LUMO + 1 and HOMO → LUMO + 3. This band can be attributed to the cis peak (S_0 $^1A_g \to S_3$ ^1A_g) as the transition reported earlier in this energy region for initiating cis/trans isomerization.[34] The molecular orbital pictures showing these transitions are shown in Figure 6. The calculated UV−vis data of **3** are also listed in Table 4. Once again, the HOMO−LUMO transition (S_0 $^1A_g \to S_2$ ^1B_u) dominates with high oscillator strength 2.5 times greater than the others. The theoretical peak observed at 483 nm (f = 1.04) involves a similar type of electronic transitions as the pyridyl adduct assigned as HOMO − 1 → LUMO and HOMO → LUMO + 1. Both of these transitions may lie under the lowest energy absorption band of **2** and **3**. A theoretical peak in the UV region was observed, this time at 287 nm. It has oscillator strength of 0.29 involving the following electronic transitions: HOMO − 2 → LUMO + 1, HOMO − 1 → LUMO + 2, and HOMO → LUMO + 2. This band can be attributed to the cis peak (S_0 $^1A_g \to S_3$ ^1A_g).

Emission Spectrum. Excitation of all-*trans*-7′,7′-dicyano-7′-apo-β-carotene, **3** at 519 nm leads to weak emission in the near-IR region which peaked at 1055 nm and is consistent with that determined by two-photon excitation.[28] The emission spectrum of **3** is shown in Figure 8. This emission is attributed to indirect population of the low-lying S_1 (2 ^1A_g) state, which results after direct population of the S_2 (1 ^1B_u) followed by internal conversion. Previous studies involving transient IR and visible spectroscopy of 8′-apo-β-caroten-8′-al and its derivatives[29,30] also lead to a possibility that the near-IR emission observed in these systems may be dependent on excitation wavelength and will be explored further.

■ SUMMARY

Two cyanine derivatives of β-apo-8′-carotenal were synthesized using the acid−base-catalyzed Knoevenagel condensation reaction. A CN stretch at 2201 cm^{-1} was observed in the infrared and at 2266 cm^{-1} in the Raman for **2** and at 2205 cm^{-1} in the Raman for **3**. Absorption maxima were red-shifted compared to the parent β-apo-8′-carotenal. The A_g and B_u symmetry orbital labels based on group theoretical calculations reported earlier[4−22] were applied to both cyano carotenoid derivatives to describe the nature of the colorful $\pi \to \pi^*$ band. DFT and TDDFT calculations established the nature and predict the location of the transitions involved in the optical spectra. Calculations revealed that the symmetry-allowed S_0 (^1A_g) → S_2 (^1B_u) transition can be assigned to the HOMO → LUMO in both cases, which are mostly polyene $\pi \rightarrow \pi^*$ in character. Weak $S_1 \rightarrow S_0$ fluorescence in the case of the dicyano derivative was found for the first time for carotenoids in the near-IR region at 1055 nm.

■ ACKNOWLEDGMENT

We thank the Wichita State University High Performance Computing Center, the Wichita State University Office of Research Administration, and the Department of Energy for support.

■ REFERENCES

(1) Polivka, T.; Herek, J. L.; Zigmantas, D.; Akerlund, H. E.; Sundstrom, V. *Proc. Natl. Acad. Sci. U.S.A.* **1999**, *96*, 4914.
(2) Frank, H. A.; Cogdell, R. *Photochem. Photobiol.* **1996**, *63*, 257.
(3) Demmig-Adams, B.; Adams, W. W. *Trends Plant Sci.* **1996**, *1*, 21.
(4) Cogdell, R. J.; Frank, H. A. *Biochim. Biophys. Acta* **1987**, *895*, 63.
(5) Young, A. J.; Britton, G. *Carotenoids in Photosynthesis*, 1st ed.; Chapman and Hall: London, 1993.
(6) Frank, H. A.; Young, A. J.; Britton, G.; Cogdell, R. J. *The Photochemistry of Carotenoids*; Klewer Academic: Dordrecht, The Netherlands, 1999.
(7) Borland, C. F.; McGarvey, D. J.; Truscott, T. G.; Cogdell, R. J.; Land, E. J. *J. Photochem. Photobiol., B* **1987**, 93.
(8) Griffiths, M.; Sistrom, W. R.; Cohen-Bazire, G.; Stanier, R. Y. *Nature* **1955**, *176*, 1211.
(9) Foote, C. S.; Chang, Y. C.; Denny, R. W. *J. Am. Chem. Soc.* **1970a**, *92*, 5218.
(10) Foote, C. S.; Chang, Y. C.; Denny, R. W. *J. Am. Chem. Soc.* **1970b**, *92*, 5216.
(11) Koyama, Y.; Kuki, M.; Andersson, P. O.; Gillbro, T. *Photochem. Photobiol.* **1996**, *63*, 243.
(12) Orlandi, G.; Zerbetto, F.; Zgierski, M. Z. *Chem. Rev.* **1991**, *91*, 867.
(13) Kohler, B. E.; Samuel, I. D. *J. Chem. Phys.* **1995**, *103*, 6253.
(14) Zoos, Z. G.; Ramasesha, S. *Phys. Rev. B* **1984**, *29*, 5410.
(15) Christensen, R. L.; Kohler, B. E. *Photochem. Photobiol.* **1973**, *18*, 293.
(16) Labhart, H. *J. Chem. Phys.* **1957**, *27*, 957.
(17) Tavan, P.; Schulten, K. *J. Chem. Phys.* **1979**, *70*, 5407.
(18) Tavan, P.; Schulten, K. *J. Chem. Phys.* **1986**, *85*, 6602.
(19) Petek., H.; Bell, A. J.; Choi, Y. S.; Yoshihara, K.; Tounge, B. A.; Christensen, R. L. *J. Chem. Phys.* **1995**, *102*, 4726.
(20) Snyder, R.; Arvidson, E.; Foote, C.; Harrigan, L.; Christensen, R. L. *J. Am. Chem. Soc.* **1985**, *107*, 4117.
(21) Granville, M. F.; Holtom, G. R.; Kohler, B. E. *J. Chem. Phys.* **1980**, *72*, 4671.
(22) Gillbro, T.; Cogdell, R. J. *Chem. Phys. Lett.* **1989**, *158*, 312.
(23) Frank, H. A.; Cua, A.; Chynwat, V.; Young, A. J.; Gosztola, D.; Wasiewelski, M. R. *Photosynth. Res.* **1994**, *41*, 389.
(24) Shreve, A. P.; Trautman, J. K.; Frank, H. A.; Owens, T. G.; Albrecht, A. C. *Biochim. Biophys. Acta* **1991**, *1058*, 280.
(25) Frank, H. A.; Bautista, J. A.; Josue, J. S.; Young, A. J. *Biochemistry* **2000**, *39*, 2831.
(26) Walla, P. J.; Linden, P. A.; Hsu, C. P.; Scholes, G. D.; Fleming, G. R. *Proc. Natl. Acad. Sci.U.S.A.* **2000**, *97*, 10808.
(27) Zimmerman, J.; Linden, P. A.; Vaswani, H. M.; Hiller, R. G.; Fleming, G. R. *J. Phys. Chem. B* **2002**, *106*, 9418.
(28) Pang, Y.; Prantil, M. A.; Van Tassle, A. J.; Jones, G. A.; Fleming, G. R. *J. Phys. Chem. B* **2009**, *113*, 13086.
(29) Pang, Y.; Jones, G. A.; Prantil, M. A.; Fleming, G. R. *J. Am. Chem. Soc.* **2010**, *132*, 2264.
(30) Pang, Y.; Fleming, G. R. *Phys. Chem. Chem. Phys.* **2010**, *12*, 6782.
(31) Evans, D. F. *J. Chem. Soc.* **1960**, 1735.
(32) Raubach, R. A.; Guzzo, A. V. *J. Phys. Chem.* **1973**, *75*, 983.
(33) Hand, E. S.; Belmore, K. A.; Kispert., L. D. *J. Chem. Soc., Perkin Trans. 2* **1993**, 659.
(34) O'Neil, M. P.; Wasielewski, M. R.; Khaled, M. M.; Kispert, L. D. *J. Chem. Phys.* **1991**, *95*, 7212.
(35) Wasielewski, M. R.; Johnson, D. G.; Bradford, E. G.; Kispert, L. D. *J. Chem. Phys.* **1989**, *91*, 6691.
(36) Cruz, A. J.; Siam, K.; Moore, C.; Islam, M.; Rillema, D. P. *J. Phys. Chem. A* **2010**, *114*, 6766.
(37) Frisch, M. J.; Trucks, G. W.; Schlegel, H. B.; Scuseria, G. E.; Robb, M. A.; Cheeseman, J. R.; Montgomery, J. A., Jr.; Vreven, T.; Kudin, K. N.; Burant, J. C.; Millam, J. M.; Iyengar, S. S.; Tomasi, J. J.; Barone, V.; Mennucci, B.; Cossi, M.; Scalmani, G.; Rega, N.; Petersson, G. A.; Nakatsuji, H.; Hada, M.; Ehara, M.; Toyota, K.; Fukuda, R.; Hasegawa, J.; Ishida, M.; Nakajima, T.; Honda, Y.; Kitao, O.; Nakai, H.; Klene, M.; Li, X.; Knox, J. E.; Hratchian, H. P.; Cross, J. B.; Adamo, C.; Jaramillo, J.; Gomperts, R.; Stratmann, R. E.; Yazyev, O.; Austin, A. J.; Cammi, R.; Pomelli, C.; Ochterski, J. W.; Ayala, P. Y.; Morokuma, K.; Voth, A.; Salvador, P.; Dannenberg, J. J.; Zakrzewski, V. G.; Dapprich, S.; Daniels, A. D.; Strain, M. C.; Farkas, O.; Malick, D. K.; Rabuck, A. D.; Raghavachari, K.; Foresman, J. B.; Ortiz, J. V.; Cui, Q.; Baboul, A. G.; Clifford, S.; Cioslowski, J.; Stefanov, B. B.; Liu, G.; Liashenko, A.; Piskorz, P.; Komaromi, I.; Martin, R. L.; Fox, D. J.; Keith, T.; Al-Laham, M. A.; Peng, C. Y.; Nanayakkara, A.; Challacombe, M.; Gill, P. M. W.; Johnson, B.; Chen, W.; Wong, M. W.; Gonzalez, C.; Pople, J. A. *Gaussian 03*, revision B.04; Gaussian Inc.: Wallingford, CT, 2004.
(38) Becke, A. D. *J. Chem. Phys.* **1993**, *98*, 5648.
(39) Lee, C.; Yang, W.; Parr, R. G. *Phys. Rev. B* **1988**, *37*, 785.
(40) Vosko, S. H.; Wilk, L.; Nusair, M. *Can. J. Phys.* **1998**, *109*, 8218.
(41) Andrae, D.; Haeussermann, U.; Dolg, M.; Stoll, H.; Preuss, H. *Theor. Chim. Acta* **1990**, *77*, 123.
(42) Stratmann, R. E.; Scuseria, G. E.; Frisch, M. J. *J. Chem. Phys.* **1998**, *109*, 8218.
(43) Bauernschmitt, R.; Ahlrichs, R. *Chem. Phys. Lett.* **1996**, *256*, 454.
(44) Casida, M. E.; Jamorski, C.; Casida, K. C.; Salahub, D. R. *J. Chem. Phys.* **1998**, *108*, 4439.
(45) Cossi, M.; Barone, V. *J. Chem. Phys.* **2001**, *115*, 4708.
(46) Barone, B.; Cossi, M. *J. Phys. Chem. A* **1998**, *102*, 1995.
(47) Cossi, M.; Rega, N.; Scalmani, G.; Barone, V. *J. Comput. Chem.* **2003**, *24*, 669.
(48) Stoyanov, S. R.; Villegas, J. M.; Rillema, D. P. *Inorg. Chem.* **2002**, *41*, 2941.
(49) Knoevenagel, E. *Chem. Ber.* **1894**, *27*, 2345.
(50) Ren, Z.; Cao, W.; Tong, W. *Synth. Commun.* **2002**, *32*, 3475.